International Journal of
MATERIALS RESEARCH

Zeitschrift für METALLKUNDE

Applied

S. Banerjee, R. Tewari, G. K. Dey
Bhabha Atomic Research Centre, Mumbai, India

Omega phase transformation – morphologies and mechanisms

Dedicated to Professor Dr. Knut Urban on the occasion of his 65th birthday

Various morphologies of the ω phase are observed in the α and the β phases of group-IV elements and their alloys where formation of this phase is induced by various means, namely, quenching from the β-phase field, isothermal annealing, under high static as well as dynamic pressure, and irradiation. The presence of various morphologies, such as ellipsoidal, cuboidal, granular or plate shapes, under different conditions is demonstrated. It is shown that various factors, including shuffling of atoms, shearing of atomic planes, long-range diffusion of solute atoms, change in volume during transformation, etc., influence the formation of different morphologies of the ω phase. The underlying mechanisms in each case are discussed. Ordered ω phases, which exist as equilibrium phases in various alloy systems, are shown as a case of superimposition of the concentration wave on the displacement wave.

Keywords: Group IV elements; Omega phase; Morphologies

1. Introduction

The occurrence of the ω-phase was first reported by Frost et al. [1] who found that aged Ti−−Cr alloys containing ~8 wt.% Cr were unexpectedly brittle. Since then, the formation of the ω phase was extensively studied, initially because of its deleterious effects on mechanical properties of β (bcc) phase titanium alloys, its influence on such physical properties as superconductivity and most importantly because the β → ω transformation exemplifies an interesting class of phase transformations.

The ω phase was encountered as an equilibrium phase in elemental Ti and Zr under static high pressures by Jamison [2]. The equilibrium phase boundaries in the pressure–temperature phase diagram have been established from a number of high-pressure studies, an excellent review of which is provided by Sikka et al. [3]. The crystallography of the α → ω transition has been studied in detail and, based on the observed orientation relationships between the phases, different mechanisms have been proposed. Recent investigations on the role of dynamic pressure (shock loading) in the α → ω or in the β → ω transition have revealed that the shock loading can result in a plate-like product which follows the invariant plane strain (IPS) criteria of the macroscopic strain.

The ω phase also appears as a metastable phase in several binary and multi-component alloys of Ti and Zr. This phase appears in Ti and Zr alloys when the stability of the β phase is enhanced by adding β-stabilising elements like V, Nb, Mo, Ta, Fe, Cr, Ni, etc. [4]. The β → ω transformation has been found to occur under two different conditions, namely, during quenching from the β-phase field and during isothermal holding at a temperature below about 773 K [5]. The kinetic characteristics of these two cases correspond to an athermal and a thermally activated process, respectively. These two processes produce two different types of morphologies suggesting the possibility of the involvement of different mechanisms. However, the underlying lattice collapse mechanism plays an important role in one form or other.

The β → ω transformation shows pronounced pre-transition effects in terms of the appearance of diffuse intensity in diffraction patterns and phonon softening along certain

wave vectors of the bcc lattice, etc. These pre-transition effects observed prior to the $\beta \rightarrow \omega$ transformation have attracted the attention of many research groups and a structural description of the pre-transition state has now emerged which is consistent with phonon dispersion relations and observed diffuse scattering [5–8]. The appearance of diffuse scattering prior to the $\beta \rightarrow \omega$ transition has prompted intense theoretical and experimental activities including inelastic neutron scattering experiments for studying the soft phonon behaviour [3, 9].

An in situ study of ω precipitation under irradiation in a high-voltage electron microscope has revealed the real-time changes in diffraction patterns and has demonstrated the progressive sharpening of ω reflections from the initial diffuse intensity distribution [10]. This observation is remarkably similar to the evolution of sharp ω reflections from the diffuse intensity distribution, which has been reported earlier in athermal $\beta \rightarrow \omega$ transformation as the temperature is progressively lowered suggesting a similarity in transformation mechanisms of the two cases.

In recent years, the structures of several ordered intermetallics based on Ti and Zr have shown the presence of chemically ordered derivatives of the ω structure. The lattice collapse mechanism of the $\beta \rightarrow \omega$ transformation, therefore, finds a much wider application in the context of the formation of these chemically ordered ω structures [11].

The ω-structure has been determined to be either hexagonal (belonging to the space group (P6/mmm) [12] or trigonal (belonging to the space group ($P\bar{3}m1$) [13]. Both structures can be generated from the parent bcc structure by simple atom movements, as will be discussed later.

The equivalent positions in the ω unit cell are:

$$\begin{aligned} &\text{A} \quad 0, 0, 0 \\ &\text{B} \quad 2/3,\ 1/3,\ 1/2 - z;\ 1/3,\ 2/3,\ 1/2 + z \end{aligned} \tag{1}$$

where $z = 0$ defines the ideal ω structure with hexagonal symmetry, $0 < z < 1/6$ defines a non-ideal ω structure with trigonal symmetry, and $z = 1/6$ defines the cubic symmetry. The two atomic sites in the ω unit cell are not equivalent. B-type atomic sites are more closely packed as compare to the A-type atomic site. Such a structure – appears like a layered structure which mimics the graphite-like layered structure – a characteristic of group-IVB elements.

The present paper describes the various morphologies of the ω phase encountered in ω-forming alloys when subjected to different treatments, namely, β-quenching, ageing, static and dynamic pressurisation, and irradiation. The underlying mechanisms of the formation of the ω phase in all these cases are discussed. The role of displacive (shuffle and shear) and diffusional atom movements responsible for the formation of different morphologies is also identified.

2. Formation and morphologies of the ω phase

2.1. Formation of the ω phase through thermal treatment

Formation of the ω phase through thermal treatment shows both types of characteristics: (a) diffusionless athermal characteristics and (b) diffusional isothermal characteristics.

Upon quenching samples of alloys, having composition in the range where martensite start temperature is lower than the ω-start temperature (M_s (ω)), from the β-phase field to a temperature below M_s (ω), the athermal $\beta \rightarrow \omega$ transformation can be initiated. The athermal nature of the transformation has been established through ultra-high quench rate ($\sim 11\,000$ K s^{-1}) experiments [13]. The complete reversibility of the transformation is further evidence for its athermal nature. All these observations suggest that this transformation can be classified as a displacive transformation.

The morphology of the athermal ω phase is generally ellipsoidal with particles aligned along one of the $<111>_\beta$ directions. Figure 1 shows a dark-field micrograph taken from the $1\bar{1}00$ reflection pertaining to the ω structure. The typical size range of the ω-particles is 2–10 nm with a separation between the particles being of the same order. A nearly homogeneous distribution of ω particles can be deduced from the micrograph. Such a morphology of the ω phase is different from the plate-like morphology (a characteristic feature of a martensitic transformation) and, therefore, the athermal $\beta \rightarrow \omega$ transformation is not categorised as a martensitic transformation in spite of its athermal and composition-invariant character.

In contrast, precipitation of the ω phase occurs in a β phase matrix of relatively concentrated alloys upon ageing at temperatures below about 773 K, which is the upper cut-off temperature for the ω-phase formation by ageing in most of the β solid solutions. The progressive increase in volume fraction and the growth of ω-particles with an increase in the isothermal holding time is indicative of a thermally activated transformation mechanism. Time-temperature-transformation (TTT) plots pertaining to isothermal ω precipitation have been experimentally generated in several alloys [14]. Both, cuboidal and ellipsoidal precipitates result in an isothermal ageing treatment. Figure 2 shows the typical cuboidal morphology of the aged ω where edges of regularly arranged cuboids are aligned along $<100>_\beta$. Usually the sizes of the ω precipitates forming by isothermal treatments are in the range of 10–20 nm.

2.2. Formation of the ω phase during electron irradiation

The volume fraction of the ω phase during irradiation depends on the balance achieved between the rate of disso-

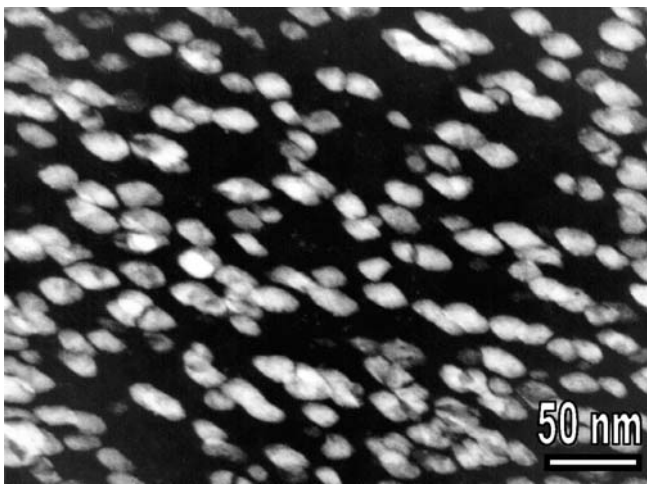

Fig. 1. Dark-field micrograph ($\boldsymbol{g} = 1\bar{1}00_\omega$) of a Zr-based alloy showing the arrangement of the ellipsoidal ω with major axes of the particles aligned along $<111>_\beta$.

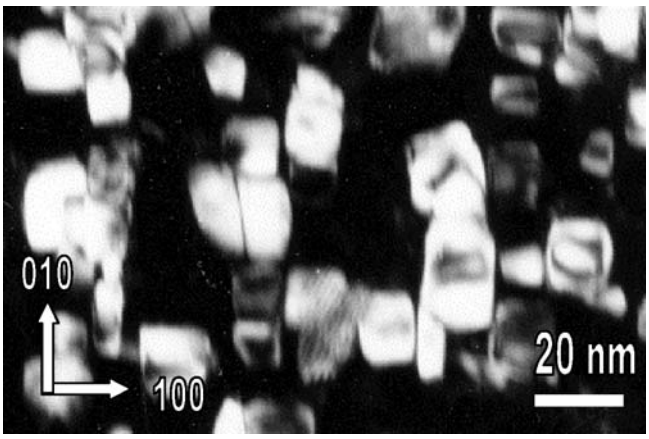

Fig. 2. Dark-field micrograph ($\boldsymbol{g} = 1\bar{1}00_{\omega}$) of a Zr-based alloy showing the arrangement of the cuboidal ω with edges of cuboids aligned along $<100>_{\beta}$.

lution of the ω particles induced by radiation and the rate of growth of the particles due to enhanced diffusion by radiation [15]. The irradiation-induced phase transformation sequence in Zr–Nb alloys has been studied by using different types of radiation like electrons, neutrons, and ions [15–17]. Figure 3 shows the real-time changes in diffraction patterns from the initial diffuse intensity distribution to progressively sharpening of ω-reflections in an in- situ study of ω-precipitation under 1 MeV-electron irradiation in a high-voltage electron microscope. The thermally activated component of the overall transformation mainly involves a solute partitioning process which accompanies the lattice collapse mechanism (as discussed in a later section). It may be noted from Fig. 3 that the ω-transformation can occur even at ambient temperature due to enhanced diffusivity under 1 MeV-electron irradiation.

Many studies have shown that during irradiation the nucleation and growth of ω occurs as a fine dispersion continuously throughout the matrix [10]. This is in contrast to that observed during ageing which produces sequential nucleation of the ω phase resulting in a periodic distribution of precipitate particles. The fine distribution of the ω phase during irradiation is obtained due to the increased number of nucleation sites provided by irradiation-induced defects as well as due to the expected enhancement in diffusion rates in the β phase.

2.3. $\alpha \rightarrow \omega$ phase transformation under high pressure

High-pressure resistivity studies on pure Zr first showed a phase transition at a hydrostatic pressure of about 6.0 GPa [18]. It has been observed [2] that the ω phase, once formed by the application of a high pressure, does not revert back fully to the α phase on removal of the pressure. A complete transformation of the ω phase into the α phase requires heating of Ti to 380 K and of Zr to 470 K for several hours after the removal of pressure.

In a way similar to the thermally induced ω-phase transformation, the pressure-induced transformation also has two modes: a shock pressure induced ω-phase transformation akin to athermal ω phase transformation, and static pressure induced ω-phase transformation analogous to the isothermal ω-phase transformation.

Typical microstructure of the ω phase generated by the static pressure loading is shown in Fig. 4. As may be noticed, the entire α grain is converted into an ω grain. The presence of curved grain boundaries suggests that grain boundaries have migrated during $\alpha \rightarrow \omega$ phase transformation.

In contrast, shock induced $\alpha \rightarrow \omega$ formation exhibits plate-like morphology (Fig. 5). Multiple variants with well-defined interfaces could be observed in the figure. Such a plate-like morphology is indicative of the involvement of a shear-type transformation. The orientation relationship between the α and the ω phases were observed to be the same in both the cases [19].

2.4. $\beta \rightarrow \omega$ phase transformation under shock pressure

The formation of the plate-like morphology of the ω phase has been reported in the $\beta \rightarrow \omega$ phase transformation in

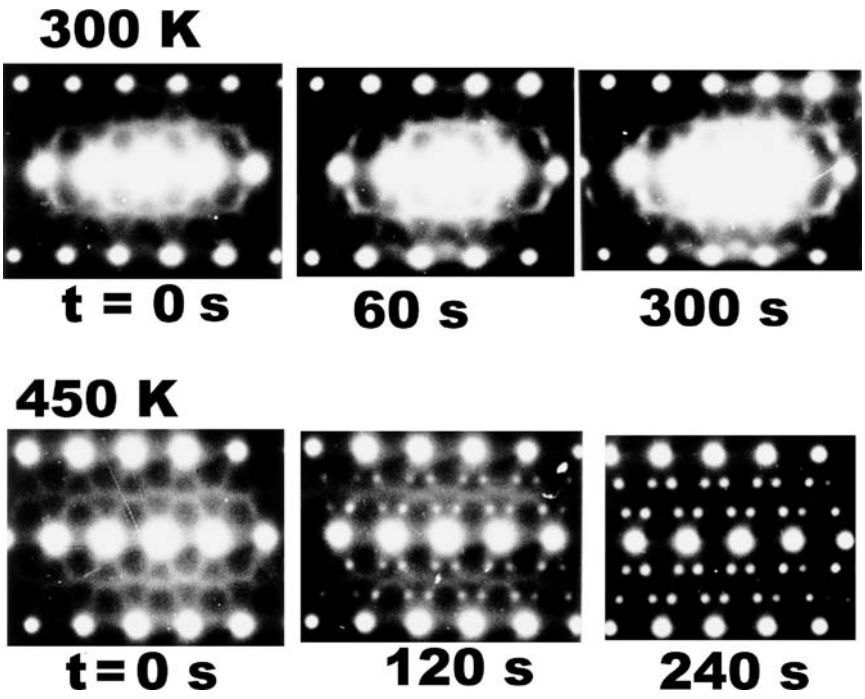

Fig. 3. SAD patterns from the $[113]_{\beta}$ zone showing the progression of the ω transformation upon irradiating samples of the Zr-20Nb alloy with 1 MeV electrons. The difference in the kinetics of the transformation with increase in temperature can be noticed.

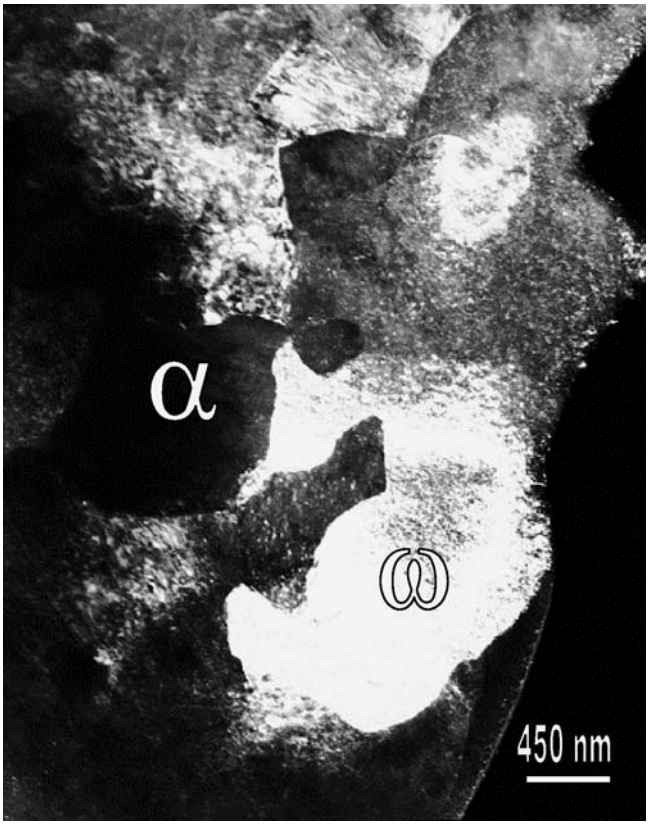

Fig. 4. Dark-field micrograph ($\boldsymbol{g} = \bar{1}\bar{1}20_{\omega}$) of pure Zr showing the transformation of the entire grain into the ω phase upon applying static high pressure 6 GPa with soaking time of 24 h.

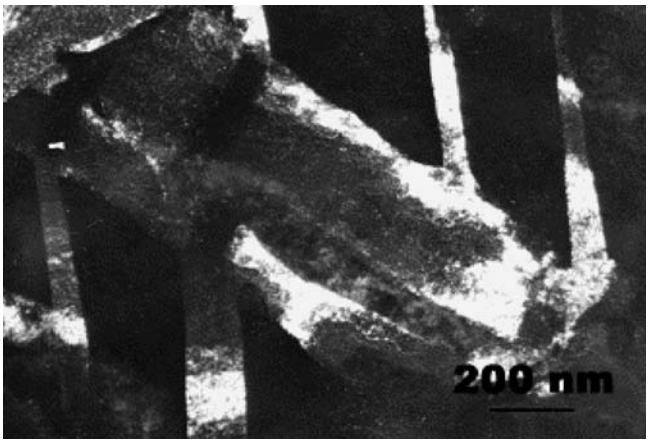

Fig. 5. Dark-field micrograph ($\boldsymbol{g} = 3\bar{3}00_{\omega}$) of pure Zr showing the plate shape morphology. The presence of multiple variants may be seen.

β-stabilized alloys by Husing et al. [20] and Dey et al. [21]. Figure 6 shows the formation of the ω phase in the Zr-20Nb alloy when the alloy was subjected to 8 GPa shock pressure. The presence of multiple variants can also be noticed from the Fig. 6a. The morphology in this case is plate-like with the $\{112\}_{\beta}$ habit plane between the ω phase and the β phase (Fig. 6b). As the duration of the shock loading is typically of the order of a few μs, diffusive atom movement is negligible. Hence the shock loading experiment, in a sense, is equivalent to the athermal treatment. The plate-shape morphology, therefore, is representative of the shear-dominated process and therefore the habit planes of the ω plates are predictable on the basis of phenomenological theory of the martensite crystallography.

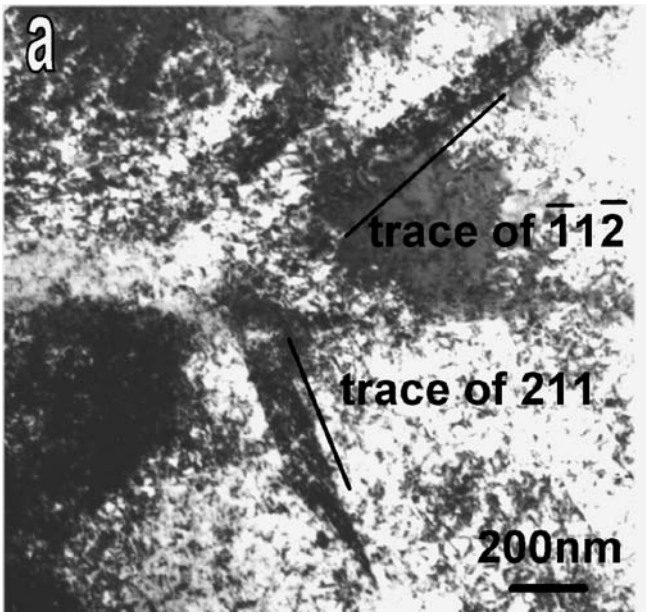

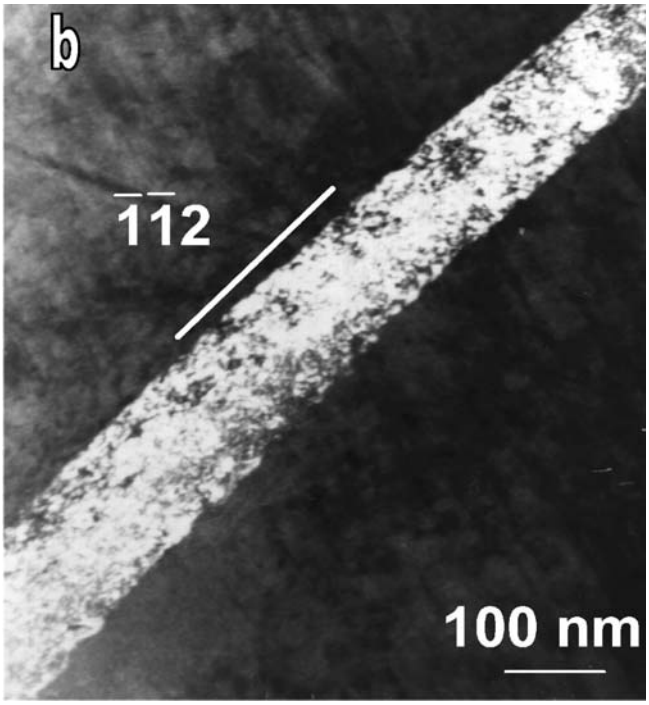

Fig. 6. Microstructure of the Zr-20Nb alloy shock loaded to 8 GPa. (a) Bright-field micrograph showing the presence of the multiple variants of the ω phase. The plate-shape morphology of the ω phase may be seen. (b) Dark-field micrograph showing the alignment of the habit plane of the ω plate along the <112> direction.

2.5. Embryonic omega

The initial stages of the formation of the ω phase manifest themselves in terms of anomalous diffusion in the bcc lattice, profuse diffuse scattering distributed in diffraction patterns, softening of the lattice vibration modes in certain wave vectors, etc. [8, 9]. Another marked difference noticed is the shift in the maxima of diffuse intensity from the ideal-ω position [6].

The existence of ω embryos in β-Zr, β-Ti, and γ-U was first proposed to explain the anomalous diffusion observed

in these metals even at temperatures higher than the $M_s(\omega)$ where a single β phase is thermodynamically stable [22]. It has been proposed that the presence of embryos may act as activated complexes for diffusion and this results in a considerable enhancement of diffusivity. These ω embryos can be visualized as defects in the bcc lattice where a jump of an atom in a <111> direction produces the configuration of the ω phase locally. Due to relatively highly correlated atomic displacements, the embryos attain significant concentration even at temperatures far above the ω start temperature. The presence of these embryos has been shown by inelastic neutron and X-ray scattering and Mössbauer studies on β-Zr at 1300 K [23].

There have been several attempts to identify the ω embryos in the parent β matrix. High-resolution electron microscopy (HREM) has recently been employed to image these embryos in ω-phase-forming alloys [21, 24]. A discrete ω region in the β matrix can be easily recognised in a HREM image. When the bcc lattice is imaged along a $<110>_\beta$ direction, due to the structural relationship between the β and the ω phases, the members of a pair of atoms in the ω structure are too close to be resolved in the image and they jointly produce a relatively bright dot contrast. Figure 7a schematically shows how, using the structural relationship between the β and the ω phases, the configuration of the ω regions develop in the β matrix, and Fig. 7b shows a high resolution image obtained from the Zr–Nb alloy. Upon comparing Fig. 7a with 7b, the presence of the ω region can easily be identified from the matrix β regions. As may be seen the short dot spacing (0.285 nm) is along either the [111] or the [11$\bar{1}$] direction and the long dot spacing (0.425 nm) is along [11$\bar{2}$] or [112]. Tilting experiments have shown that the different variants of commensurate ω fill the entire volume without leaving any β region untransformed.

It has been shown that the pre-transition effects associated with the β → ω transformation can be attributed to the ω-like atomic arrangement, which is created locally at

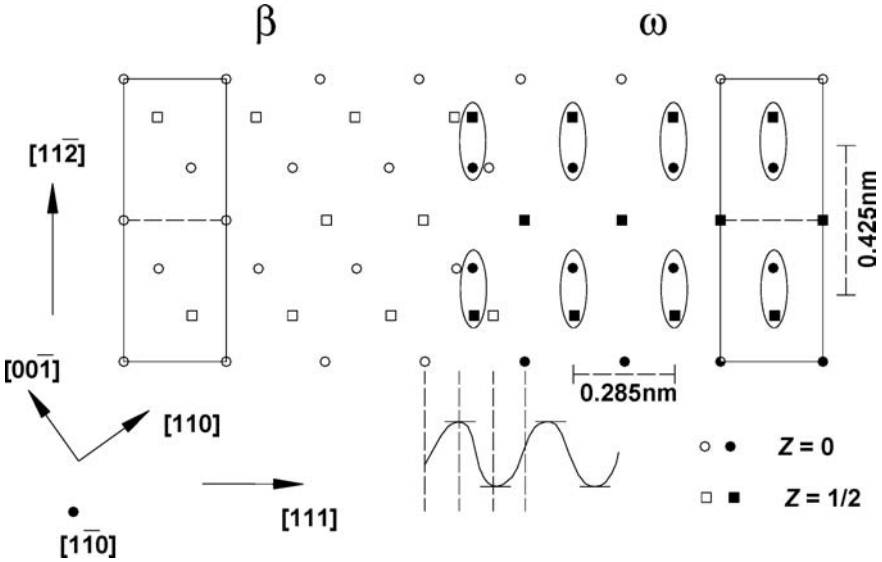

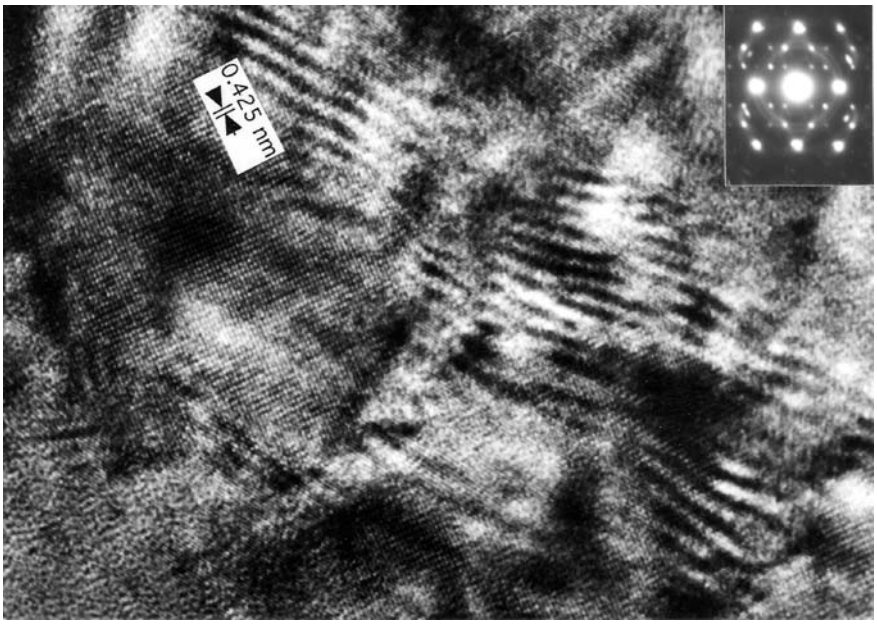

Fig. 7. (a) Schematic representation of formation of the ω lattice from the β lattice through the collapse mechanism. Two atoms within an ellipse come closer than the resolving power of the TEM and therefore appear as bright dots. (b) HREM image showing the above two phases.

nanometer scale in the bcc lattice along the $<111>_\beta$ direction prior to the transformation [24]. HREM was carried out to identify the nature of the instability in the β phase, which is responsible for the diffuse intensity maxima in the electron diffraction patterns. Figure 8 is an HREM image from a region showing a diffuse intensity pattern (shown inset in the figure) taken along the [110] direction. In addition to the [110] lattice fringes, it was possible to see the presence of strings of white dots (indicated by arrows) in some places, mostly inclined to the {111} by about 10°. These regions essentially contain the ω-like linear defects in the bcc lattice. In this regard, the observations made in Fig. 8 are very similar to those made by Schryvers and Tanner [24] in a Ti–Mo alloy. In order to correlate these strings with the embryonic ω it is necessary to understand the mechanism of the transformation. Therefore this issue will be addressed in detail in the next section.

3. Mechanisms of transformation

3.1. β → ω transformation

The mechanism of the β → ω transformation can be viewed as a collapse of (222) lattice planes of the bcc structure in a sequence shown in Fig. 9, where the lattices of the β (Fig. 9a) and the ω phases (Fig. 9b) have been shown oriented in accordance with the experimentally determined orientation relationship between the β and the ω phases [5, 7, 8]:

$$\{111\}_\beta \,//\, (0001)_\omega;\ <1\bar{1}0_\beta> \,//\, <11\bar{2}0>_\omega \qquad (2)$$

The three-layer stacking sequence (0, 1, 2 . . .) of {222} planes changes to the two layer stacking sequence of the ω structure when the planes are collapsed in the middle (marked as 1.5) keeping the 0 and 3 planes undisplaced. Such a periodic displacement of the $\{222\}_\beta$-type planes can be represented by a longitudinal displacement wave with wavelength, $\lambda = 3\ d_{222}$, and a corresponding wave vector, $\boldsymbol{K}_\omega$, equal to $2/3<111>^*$ (where $<111>^*$ is a vector in the reciprocal space) (Fig. 9d). The merit of this description lies in the fact that it can be applied to partial collapse situations also by varying the amplitude of the displacement wave, the amplitude being directly related to the order parameter, η.

Figure 10a–d show the edge-on arrangement of the {222} planes. In the case when a wave with an equal but negative amplitude (hence, negative η) (Fig. 10c), is induced in the bcc lattice, the anti-omega (-ω) structure is produced in which the two collapsing layers of the bcc lattice are displaced towards the undisplaced layer and thus generate a three-layer collapse (Fig. 10c and f). The fact that the anti-omega (-ω) configuration is not structurally equivalent to the omega (ω) configuration makes the free energy versus η plot asymmetric around $\eta = 0$. Cook [25] has put forward this symmetry argument to justify that the β → ω transition is of first-order character. This has been experimentally vindicated by the observation of the coexistence of the two phases β and ω.

3.2. Athermal β → ω transformation

In order to account for the characteristic features associated with the β → ω transformation, such as: (i) strong pre-transition effects in terms of profuse diffuse scattering and lattice softening and (ii) fine particulate ellipsoidal morphology of athermal ω, which always remains finely di-

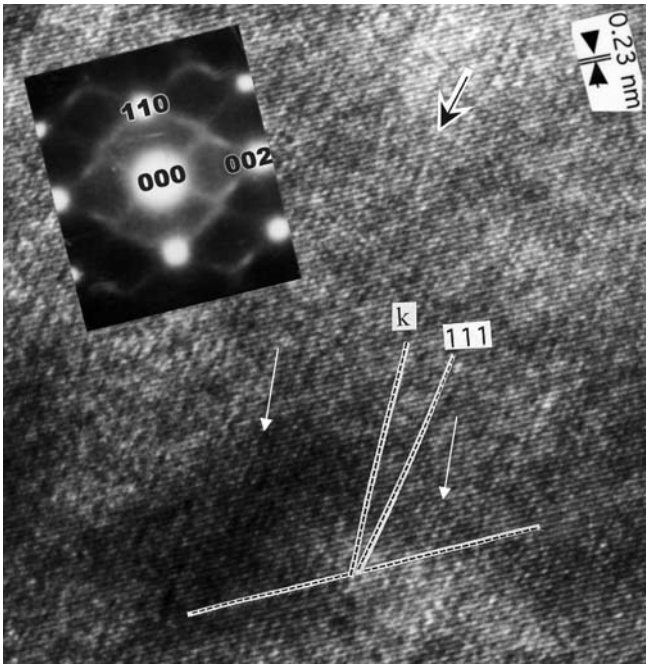

Fig. 8. High-resolution image taken from the [110] zone axis showing lattice image of the {110} planes. In addition, short strings of white dots of incommensurate ω can also be observed in the micrograph. Such strings of dots are due to the formation of the embryos of the ω phase resulting out of the collapse of the $\{111\}_\beta$ planes locally. Alignment of these white dots is close to the $<111>_\beta$ direction. The vectors shown in the image are defined in Fig. 12.

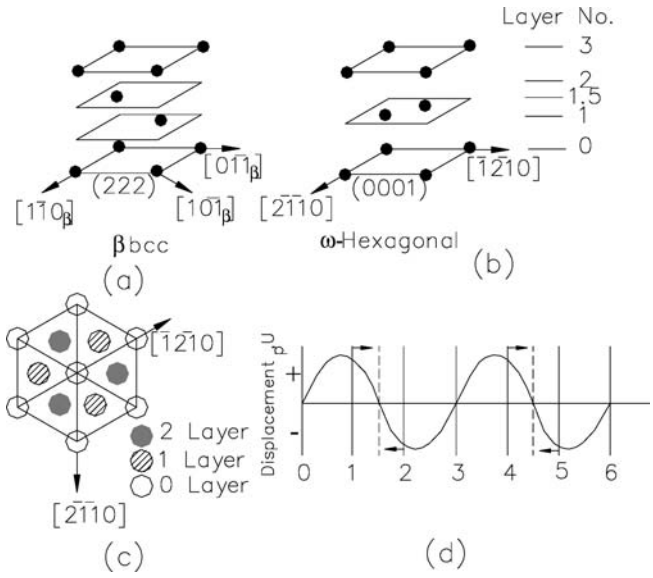

Fig. 9. (a) Planar arrangement of the $\{222\}_\beta$ atomic planes in the bcc lattice. The 0, 1, 2, . . . sequences of atomic plane arrangements can be seen. (b) The planar arrangement of the $(0001)_\omega$ atomic planes in the ω lattice. As can be seen the ω-lattice can be obtained from the bcc lattice by collapsing a pair of planes (1 and 2) to the middle (marked as 1.5) while keeping the third one (0 and 3) undisturbed. (c) Completely collapsed {222} planes form a six-fold symmetry, whereas an incomplete collapse forms a three-fold symmetry along the <111> axis. (d) The displacement of {222} planes can also be visualized in terms of a sinusoidal displacement wave where upward movement is seen as a positive displacement and downward as negative displacement.

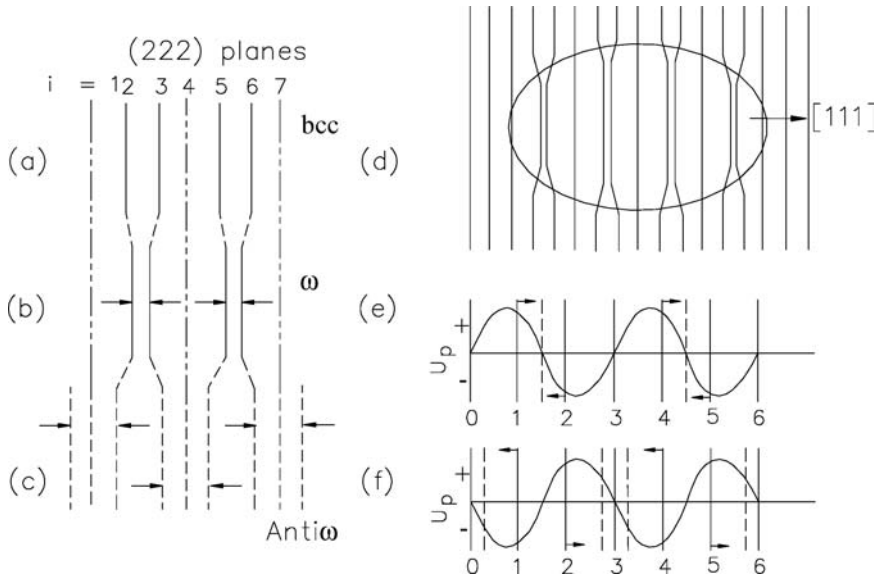

Fig. 10. Two possibilities of the collapse of the $\{222\}_\beta$ planes are shown. (a) Represents arrangement of the $\{222\}_\beta$ planes, viewed on edge, in the bcc lattice. One possibility of collapse is shown in the (b) where two planes have collapsed (planes 2 and 3, 5 and 6) and in (c) where three planes collapsed (marked as 3, 4, 5). The two-plane-collapse produces the ω structure whereas the three-plane-collapse produces anti-ω. (d) The collapsed regions in the bcc lattice showing the ω region are marked by an ellipse. This schematic provides a clue for the ellipsoidal morphology of the ω-phase. (e) and (f) are the wave representation of the ω and anti-ω structures. The final positions of the planes are shown by broken lines.

vided (typically less than 5 nm in diameter), Cook [25] invoked a "wave packet" structure associated with a spread of wave vectors, from $\boldsymbol{K}_m$ to $\boldsymbol{K}_\omega$, where $\boldsymbol{K}_m$ is the wave vector associated with the structure which derives its stability only from the harmonic term of the free energy expansion. The modulated structure arises due to the difference between $\boldsymbol{K}_m$ and $\boldsymbol{K}_\omega$ resulting in a long periodic structure consisting of wave packets of ω uniformly distributed in the β matrix. Such a structure is associated with lower free energy than the ideal ω structure.

3.3. Formation of embryonic ω

Figure 11 shows the presence of minima at positions other than $\eta = 0$ in the ΔG versus η plots in the temperature range, $T_m > T > T_o(\omega)$, where T_m represents the highest temperature at which the ω-like fluctuations were noticed and $T_o(\omega)$ is the temperature where the free energies of the β and the ω phases were equal for a given alloy composition. The minima correspond to the presence of a metastable state which can be described as "ω-like fluctuations". These minima allow the system to locally attain the structure pertaining to the order parameter and remain there for a duration longer than the inverse of vibrational frequency of the atoms. At higher temperatures, these local configurations, which appear as linear defects along <111>, remain uncorrelated, each row diffracting independently. However, with a temperature approaching the transformation temperature, the correlation among these local configurations improves along with an increase in population of such fluctuations, which finally results in discrete ω particles when the temperature is lower than the transformation temperature. Upon athermal quenching from the β-phase field these local arrangements, which are present in the β matrix at any given time, can be frozen-in at room temperature. These structures are responsible for profuse diffuse scattering observed in the as-quenched microstructures [6, 21, 24].

In order to explain the diffuse intensity maxima, the idea of one dimensional ω-like displacements has been introduced in models (for example by Sinkler and Luzzei [26]). Schryvers and Tanner [24] have shown in HREM images that the diffuse intensity in the diffraction patterns corresponds to the presence of linear arrangements of atoms of several nanometers in length which correspond to the omega configuration. Their structural model incorporates the deviation of these linear atomic arrangements from the <111> direction (marked in Fig. 8). The linear omega configuration is generated by shifting the atoms in the bcc structure by incorporating a phase shift [24]. These authors have simulated the HREM images and compared it with the observed images in the case of Ti–Mo alloys. The HREM image shown in Fig. 8 is very similar to that reported by Schryvers and Tanner [24].

The atomic shuffles required in the bcc lattice to produce the one dimensional omega structure is shown schema-

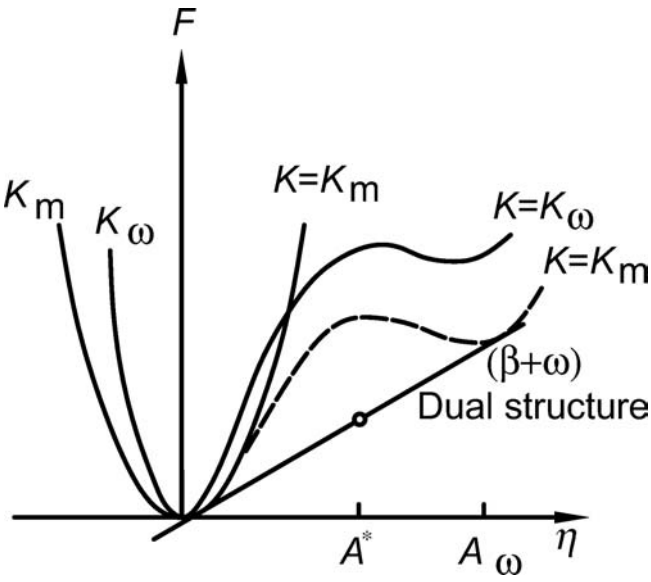

Fig. 11. Schematic representation of the free energy of two (β and ω) phases as a function of the order parameter. The asymmetric nature of the free energy curves represents the first-order nature of the ω-phase transformation. The figure represents a situation where the temperature is above the $T_o(\omega)$ temperature. A local minimum of the free energy allows the system to temporarily attain the ω structure with a life time larger than the vibration frequency. Two-phase structures are always energetically more favourable compared to completely single phase.

tically in Fig. 12. In the case of local fluctuation, atoms in the bcc lattice come closer to the limit of resolution of TEM and, therefore, appear as dots. Figure 12a shows modulations in one direction. In such a case, all dots are completely aligned along the <111> direction. In contrast, Fig. 12b shows an arrangement in which an array of ω modulation has deviated from the <111> direction by a phase shift arising due to the interaction of different variants of the ω configuration possible in the β lattice. As the choice of the collapsing plane is completely random and local, a random arrangement of the ω fluctuation emerges and when these dots are joined by a vector it deviates from the <111> vector by nearly 10°. Upon comparing this figure with the HREM image shown in Fig. 8, it is possible to find such strings of dots which were aligned close to <111> with deviations up to 10° from the <111> direction. Several such strings can also be seen along the other <111> directions in the HREM image shown in Fig. 8.

3.4. Isothermal β → ω transformation

The lattice collapse mechanism of the β → ω transformation involves only shuffling of atoms and does not produce any macroscopic shape strain. When such a mechanism is operative, the product and the parent phases can maintain complete coherence along the entire interface. For such a transformation there is no requirement of the strain energy minimisation by a proper choice of the product morphology. The morphology so developed is shown in Fig. 10d. The $\{111\}_\beta$ planes are shown in this figure at the edge-on position and the superimposed ellipse shown in the figure represents the ω particle. The continuity of the planes can be maintained across all the interfaces and the extent of collapse, the latter reducing from the center to the surface of the particle give rise to ellipsoidal morphology.

In view of the fact that the β phase in most of the ω-forming alloys exhibits a tendency for phase separation, spinodal decomposition often precedes the β → ω phase transformation during isothermal heat treatments. Spinodal decomposition partitions the β phase into solute-rich and solute-lean regions and composition modulation occurs only in elastically soft <100> directions. The formation of the ω phase, therefore, follows the same configuration and ω particles decorate the <100> fluctuation in composition with the edges of the interfaces aligned along the <100> direction of the bcc matrix [27]. Under special circumstances where strain associates with the transformation, ω particles assume an ellipsoidal morphology and the particles remain small in size due to the transformation strain.

3.5. Shock-induced β → ω transformation

In the case of shock loading, a macroscopic shape strain is superimposed on the β → ω transformation and the choice of the interface is restricted by the criteria of minimisation of the interfacial energy and the strain energy associated with the transformation. For example, in the martensitic transformation the strain energy contribution dominates and the invariant plane strain (IPS) condition is satisfied. The surface energy term dictates the selection of habit planes. In several diffusional transformations the invariant line (IL) vector, lying along the habit plane, which defines

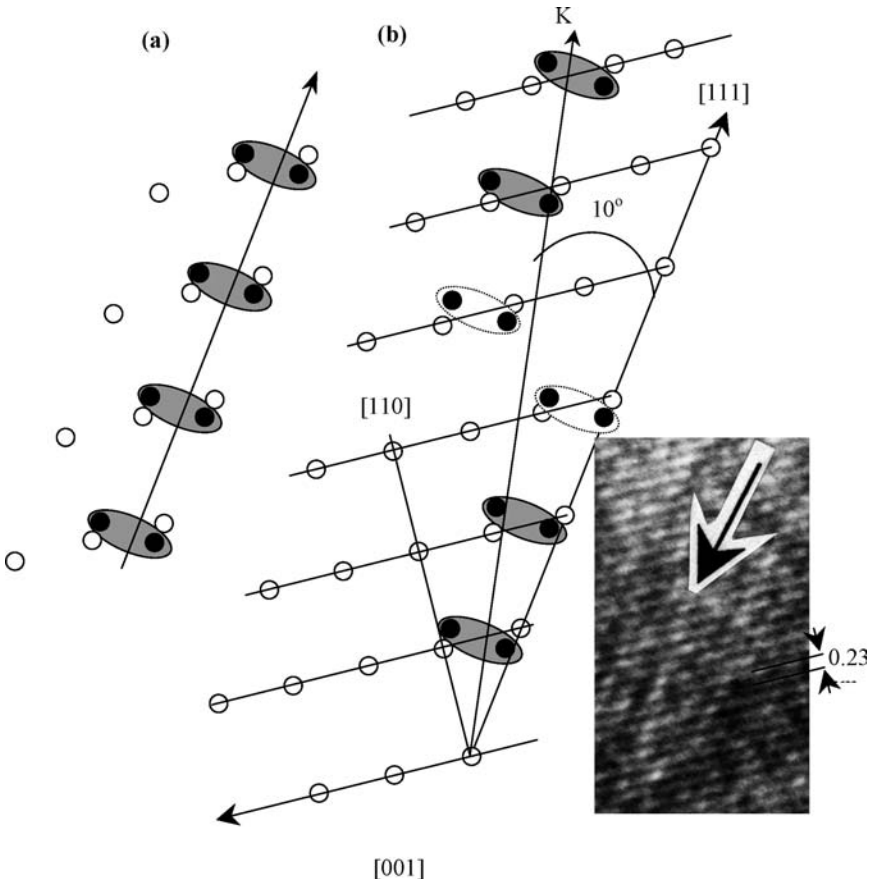

Fig. 12. Schematic representations of changes in the local arrangements of atoms in the bcc lattice in order to achieve the ω-configuration. The collapse of {111} planes of bcc at local level brings the two atoms closer than the resolution of a TEM. (a) shows the arrangement of atoms in a case when only one single variant of the ω phase is present. If such a structure prevails in the whole region, the alignment would be exactly along the <111> direction. (b) A configuration where two variants interact. As a result the vector joining all the spots would be rotated by 10° with respect to the <111> vector. Inset shows a magnified view of a section taken from Fig. 8.

the primary growth direction, is essentially due to the minimisation of the strain energy associated with the transformation [28].

In a similar fashion, if there is a volume change involved during the $\beta \rightarrow \omega$ transformation and if the external stress involved has a shear component, the choice of the interface is not completely random. In fact, it has been shown under these circumstances that the product ω phase has a plate-shape morphology and the habit plane between the parent β and the ω phases can be predicted using the phenomenological theory of martensite formation [29]. Using this theory, Dey et al. [21] derived the Bain strain and also the macroscopic shape-strain matrix. The predicted habit plane was very close to the experimentally determined (121) habit plane (Fig. 6b). The observation of $\{112\}_\beta$ planes as habit planes of the ω phase is suggestive of the fact that the $\beta \rightarrow \omega$ transformation involves a shearing of the β lattice along a $\{112\}_\beta$ plane.

Figure 13 shows that a macroscopic shear on the $\{112\}_\beta$ plane along a <111> direction, superimposed with atomic shuffles, can produce the ω structure. Since the macroscopic deformation is a simple shear, the invariant plane, which is the contact plane between the two phases, is the shear plane itself. In this case, the lattice invariant shear operates for the macroscopic strain to satisfy the invariant plane strain condition. It is possible to define a homogeneous shear on the (112) plane with a magnitude of cot $\phi/2 = 0.767$, where ϕ is defined as the angle between the $[\bar{1}\bar{1}2]$ and the [110] directions. The $[\bar{1}\bar{1}0]$ direction (η_2) remains undistorted after this shear because the shear plane is $(\bar{1}\bar{1}2)$. Using the well-known geometrical relation of homogeneous deformation, which is very commonly used in the case of deformation twinning, the magnitude of shear can be determined. The homogeneous deformation comprising the shear part alone produces a lattice, which is indistinguishable from the β parent lattice. When atom shuffles similar to those shown in Fig. 13 are superimposed on the homogeneous deformation, the ω structure is generated. The lattice correspondence between the β and ω lattices remains the same as that encountered when a longitudinal displacement wave is introduced in the β lattice. This equivalence, generated by (i) a combination of shear and shuffle and (ii) a longitudinal displacement wave, can be appreciated from Fig. 13. Since any specific {112} plane contains only one $<111>_\beta$ direction, a single orientational variant of the ω structure can be produced within a single {112} plate.

In short, the deformation produced by a shock wave in the bcc lattice develops a tendency for the shear of the {112} planes where the formation of the ω structure occurs when the shuffle process is superimposed on the shear deformation. The axis of the shear direction decides the choice of the variant for the <111> direction contained in the specific {112} plane and, therefore, plate-shaped single variants of the ω-phase emerge in the shock deformed β phase.

3.6. $\alpha \rightarrow \omega$ transformation

The $\alpha \rightarrow \omega$ phase transformation remained the realm of the high pressure transformation, where TEM examinations carried out on the pressurised samples showed orientation relationship between α and ω producing two crystallographically non-equivalent variants [30–33].

Several studies, including both shock and static loading experiments, confirmed the presence of these two orientation relationships. Based on these crystallographic analyses Usikov and Zilbershtein [30] proposed a mechanism in which the $\alpha \rightarrow \omega$ phase transformation proceeds through an intermediate bcc configuration. In Ti–V alloys, high-pressure studies revealed the presence of the β phase which was taken as direct evidence of the presence of the intermediate structure [31]. But, Rabinkin et al. [32] after examining pressure-treated Zr samples by TEM, observed ellipsoidal morphology similar to that observed in the as-quenched samples and proposed a diffusionless mechanism in which the formation of the ω phase occurs directly from the α phase without involving any intermediate structure.

The influence of the exposure time at a constant pressure at ambient temperature on the $\alpha \rightarrow \omega$ transition has been systematically studied and the time dependence of the

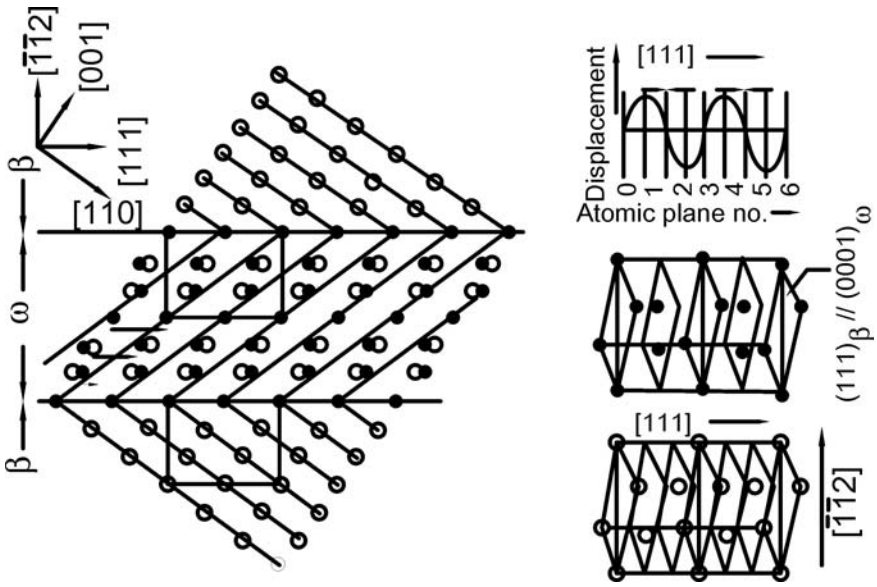

Fig. 13. Planar stacking of the $\{222\}_\beta$ planes of the bcc lattice (shown by open circles). If the shuffling of the atoms is superimposed during the shearing of the $\{222\}_\beta$ planes the ω-structure is produced (shown by the filled circles). The orientation relationship between the two structures remains the same as shown in Fig. 10. The two lattices are also shown. In order to show the equivalence between the shear model and the wave model, the displacement wave is also shown in the inset.

growth of the ω volume fraction has been established. The rate of the ω transformation as a function of pressure shows a peak (Fig. 14) [3] analogous to that observed in the nucleation-rate versus temperature plots pertaining to isothermal martensitic transformations (in which nucleation is thermally activated, but the growth is athermal). The time-dependent nature of the pressure-induced $\alpha \rightarrow \omega$ transformation suggests that there exists a barrier, possibly that of the nucleation step, which can be overcome by thermal activation. The nucleation step involves the growth of quasistatic ω embryos to the critical size by a thermally-assisted diffusion process. After attaining the critical size, the nuclei grow spontaneously in an athermal manner. The observed peak in the rate versus pressure plot is consistent with the fact that the driving force increases while the diffusivity decreases with increasing pressure. Figure 4 shows a microstructure where the sample was soaked for longer (~ 24 h), unlike samples soaked only for 4 h to 8 h in some previous studies [32, 33]. In contrast to the particulate morphology observed in the short-duration experiments, complete conversion of the α grain into the ω grain suggests a time-dependent nature of the $\alpha \rightarrow \omega$ transformation. The curved boundaries of the ω phase provide evidence of grain boundary migration during the $\alpha \rightarrow \omega$ phase transformation.

Recently, Jyoti et al. [19] carried out detailed crystallographic analyses on the samples, which were shock as well as static loaded, and showed that, although the morphology of the ω phase is different in both the cases, the orientation relationship is the same in either case. In order to estimate the total strain involved in the $\alpha \rightarrow \omega$ phase transformation in which bcc configuration appears as an intermediate step, Jyoti et al. calculated the homogeneous strain (ε_1) and a shuffle strain (ε_2) required to transform α into β and an additional shuffle strain (ε_3) required to transform β into ω. In contrast, during shock loading the shear stress is a dominant component and hence the $\beta \rightarrow \omega$ transformation may occur in a way similar to the one shown in the Zr-20Nb alloy [21] and under such conditions a plate-shape morphology of the ω phase is expected.

4. Ordered derivatives of the ω phase

The displacive transformation mechanism of the $\beta \rightarrow \omega$ transformation that has been considered so far, has always been treated by ignoring the decoration of different atoms on the different lattice sites. The formation of ordered omega structures can be viewed as a superposition of composition and displacement modulations. In fact, diffuse scattering, a characteristic of a pre-transition effect, was observed prior to the ordered ω transformation [34].

Presetyo et al. [35] have reported the formation of the displacive ω-like transformation in β-brass. The transformation from β to the ordered omega structures has been encountered in several systems like Ni–Al, Zr–Al, Zr–Al–Nb, Ti–Al–Nb alloys, etc. Banerjee et al. [36] have reported the occurrence of the $\beta \rightarrow B8_2$ in the rapidly solidified Zr-27 at.% Al alloy, which underwent prior spinodal decomposition. Figure 15 shows the as-rapidly-solidified microstructures of Zr–Al based alloys where cuboids of the ordered ω phases are seen aligned along the <100> direction. Spinodal decomposition in these alloys resulted in the formation of Al-rich nodes at the junction of the <100> modulations, which subsequently transformed into a single Zr_2Al particle suggesting a homogeneous transformation where formation of the particle has not experienced any nucleation barrier. The matching of the size of the particle with the spinodal wave length, which is 20 nm, could be taken as evidence for the above argument.

The ordered ω-phase transformation in this case appears to involve the following steps in the overall transformation:

(i) Congruent solidification of the liquid phase into the supersaturated β phase.
(ii) Development of the concentration fluctuation in the supersaturated β phase.
(iii) Formation of the ordered ω phases in the solute-rich regions.
(iv) Transformation of the metastable phases into the relatively stable phases.

While examining the $B2 \rightarrow B8_2$ transformation in ternary Ti–Al–Nb alloys, Bendersky et al. [11] have encountered a metastable intermediate phase, ω″, which is of a lower symmetry than either of the initial B2 and the final $B8_2$ structures. The ω″ phase is characterized by partially collapsed (111) planes and is reordered relative to the B2 phase (Fig. 16). The occurrence of a partially collapsed structure essentially indicates a strong coupling between the chemical (replacive) and the displacive ordering processes.

It has been shown that the $\beta \rightarrow B8_2$ structural transition would require a combination of the collapse of the layers

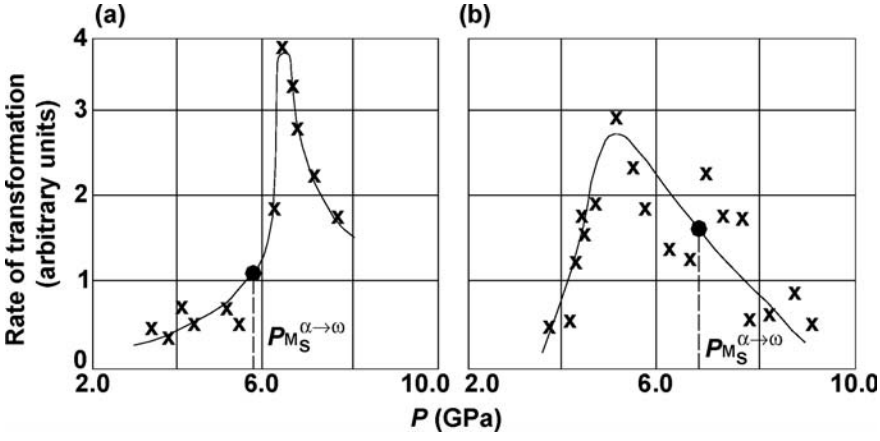

Fig. 14. The rate of ω phase transformation with pressure shows a peak in between (a) 6 and 7 GPa in case of Ti and (b) 5 and 6 GPa in case of Zr. The theoretically calculated start pressure for the $\alpha \rightarrow \omega$ phase transformation is also shown.

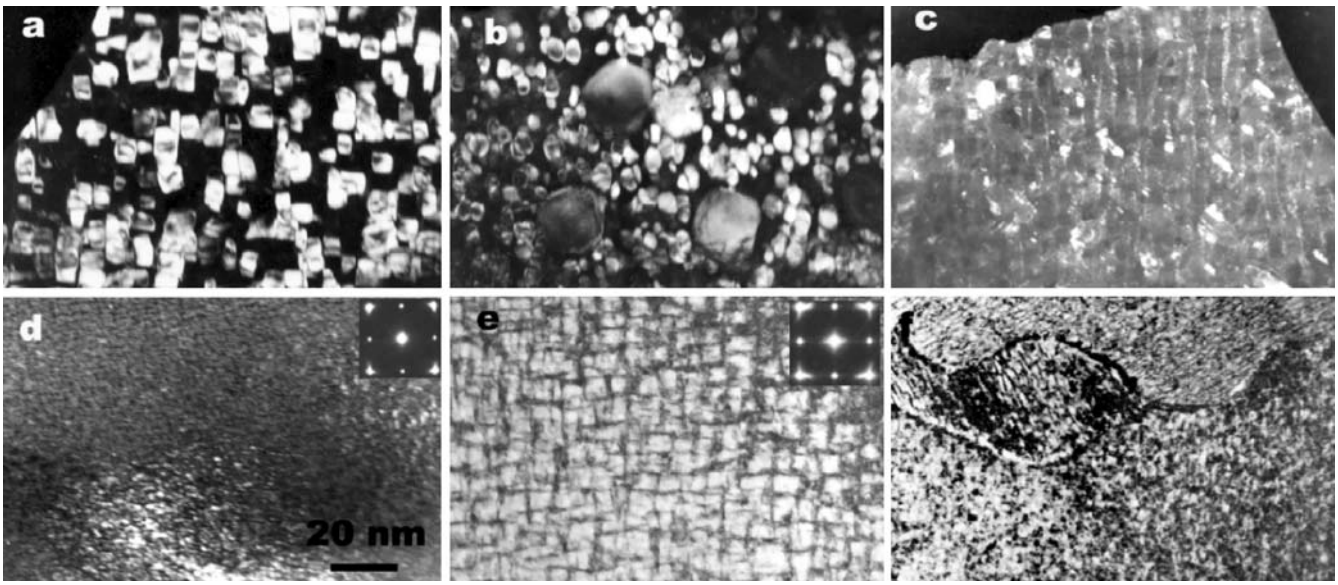

Fig. 15. Rapidly solidified microstructure of Zr–Al binary and ternary alloys. (a) Rapidly solidified Zr_3Al-3Nb alloy. The dark-field micrograph shows the presence of $D8_8$ cuboidal particles imaged using $\boldsymbol{g} = (1\bar{1}00)_\omega$. (b) Dark-field micrograph ($\boldsymbol{g} = 1\bar{1}00$) of the bimodal distribution of the $D8_8$ phase. A tendency of $<100>_\beta$ alignment of the cuboidal phase is noticed. (c) Matrix β phase of the rapidly solidified Zr_3Al–3Nb alloy with a distribution of fine ω particles exhibiting bright contrast with $\boldsymbol{g} = (031)_\beta$. (d) Bright-field image showing modulations along $<100>_\beta$ directions in the rapidly solidified Zr_3Al alloys. (e) Bright-field image showing an increase in the modulations along $<100>_\beta$ directions upon aging the rapidly solidified Zr_3Al alloys. Please note a change in the diffuse intensity in the SAD patterns shown in the insets of (d) and (e). (f) Bright-field image showing changes in the $<100>_\beta$ modulations upon moving from one grain to another.

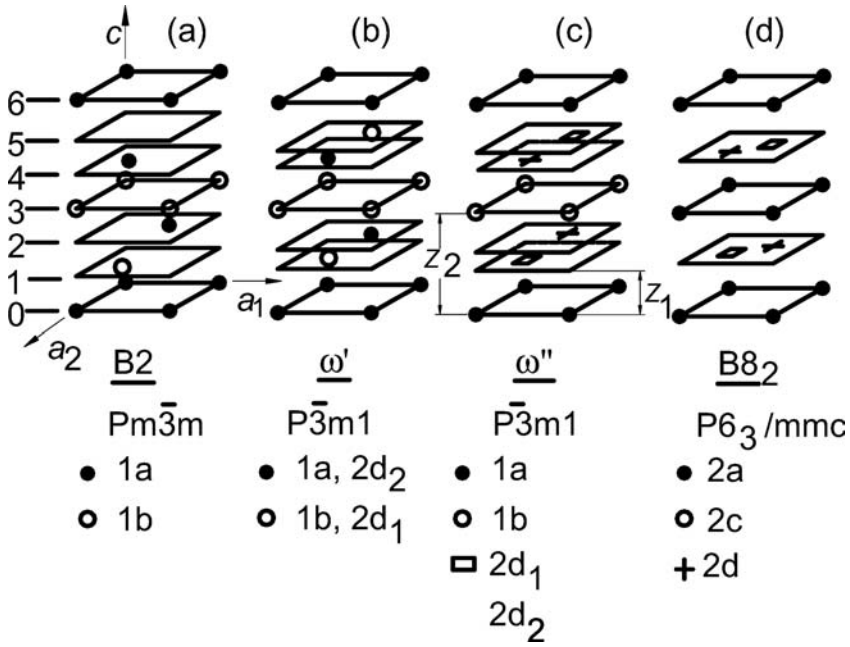

Fig. 16. The lattice correspondence between ordered derivatives of bcc (B2) and the ordered ω structures. Different atomic sites and arrangements of the $(222)_{bcc}$ planes is shown. Gradual and complete collapse of the two pairs of the (222) planes and chemical ordering leading to changes in structural symmetry are shown.

(1, 2; 4, 5; etc.) and a chemical ordering (Fig. 16). The fact that such a lattice correspondence exists in several real systems has been demonstrated [11, 26, 36]. Based on this correspondence the lattice parameters, a and c, of the $B8_2$ phase can be expressed in terms of the lattice parameter, a_β,

$$a_B = \sqrt{2}a_\beta; \quad c_B = 6d_{222} = \sqrt{3}a_\beta$$

where B stands for the $B8_2$ structure. Substituting the extrapolated values of a_β for Zr-33 at.% Al and for Ti-33 at.% Al, the lattice parameters of Zr_2Al and Ti_2Al work out to be the following:

For Zr_2Al: $a = 0.4852$ nm $\quad c = 0.5942$ nm
For Ti_2Al: $a = 0.4580(3)$ nm $\quad c = 0.5520(4)$ nm

Tewari et al. [37] have observed the presence of yet another ordered ω structure which has the $D8_8$ structure (prototype Mn_5Si_3). Bendersky et al. [38] have also reported such a structure in ternary Ti–Al–Nb alloys.

This structure with a hexagonal unit cell possesses 18 Wyckoff positions (Table 1). The stacking sequence and

Table 1. Wyckoff positions, site occupancy, interplanar spacings, and the relative peak intensities for Zr_5Al_4 (Ga_4Ti_5 type) and Zr_5Al_3 (Mn_5Si_3 type) phases.

Prototype structure	Wyckoff position/occupancy	*hkl*	*d* spacing (nm) (λ = 0.1544 nm)	relative intensity
Ga_4Ti_5	2(b) 000 Al	100	0.727	25
(Zr_5Al_4)	4(d) 1/3 2/3 0 Zr	110	0.420	0
	$6(g_1)$ x_1 0 1/4 Zr	200	0.363	62.5
	$6(g_2)$ x_2 0 1/4 Al	111	0.343	62.5
	$x_1 = 0.23$, $x_2 = 0.60$	002	0.297	100
Mn_5Si_3	2(b) 000 vacancy	100	0.727	0
(Zr_5Al_3)	4(d) 1/3 2/3 0 Zr	110	0.420	66
	$6(g_1)$ x_1 0 1/4 Zr	200	0.363	100
	$6(g_2)$ x_2 0 1/4 Al	111	0.343	66
	$x_1 = 0.23$, $x_2 = 0.60$	002	0.297	100

the lattice correspondence in the $D8_8$ structure are compared with those in the B2 structure in Fig. 17. This figure also depicts the lattice correspondence between these two structures. Based on this correspondence the lattice parameters of the $D8_8$ phase are related to that of the ordered β phase (B2 structure) as:

$$a_{D8_8} = \sqrt{6}a_\beta \text{ and } c_{D8_8} = 6d_{222,\beta} = \sqrt{3}a_\beta$$

In the case of Zr_5Al_3, the substitution of the corresponding a_β (= 0.3455 nm) value yields the *a* and *c* parameters of the $D8_8$ phase as 0.8464 nm and 0.5984 nm, respectively, which are fairly close to the experimentally obtained lattice parameters (*a* = 0.845 nm and *c* = 0.5902 nm) of the equilibrium Zr_5Al_3 phase. Figure 17 shows that the $D8_8$ structure also can be generated from the B2 structure by a combination of lattice collapse and chemical ordering. The pairs of {222} planes which collapse in the $B8_2$ and in the $D8_8$ structure are essentially the same. In case of the $D8_8$ structure an ordered array of vacancies is necessary in those B2 planes which remain undisplaced during the collapse. This is essential for meeting the stoichiometric requirement. The difference between the $B8_2$ and the $D8_8$ structures lies in whether the 2(b) positions are occupied by Zr atoms or vacant (Fig. 18). The fact that 2 vacancies for 18 atom positions per unit cell are required for the formation of the $D8_8$ structure necessitates the retention of a high concentration of vacancies in the parent B2 structure and an ordered arrangement of these vacancies. If the 2(b) positions are occupied with Al atoms, a stoichiometry of Zr_5Al_4, having a Ga_4Ti_5 structure, is attained.

Bendersky et al. [11] have constructed the symmetry tree showing symmetry changes that occur during partial and complete lattice collapse associated with the β → ω

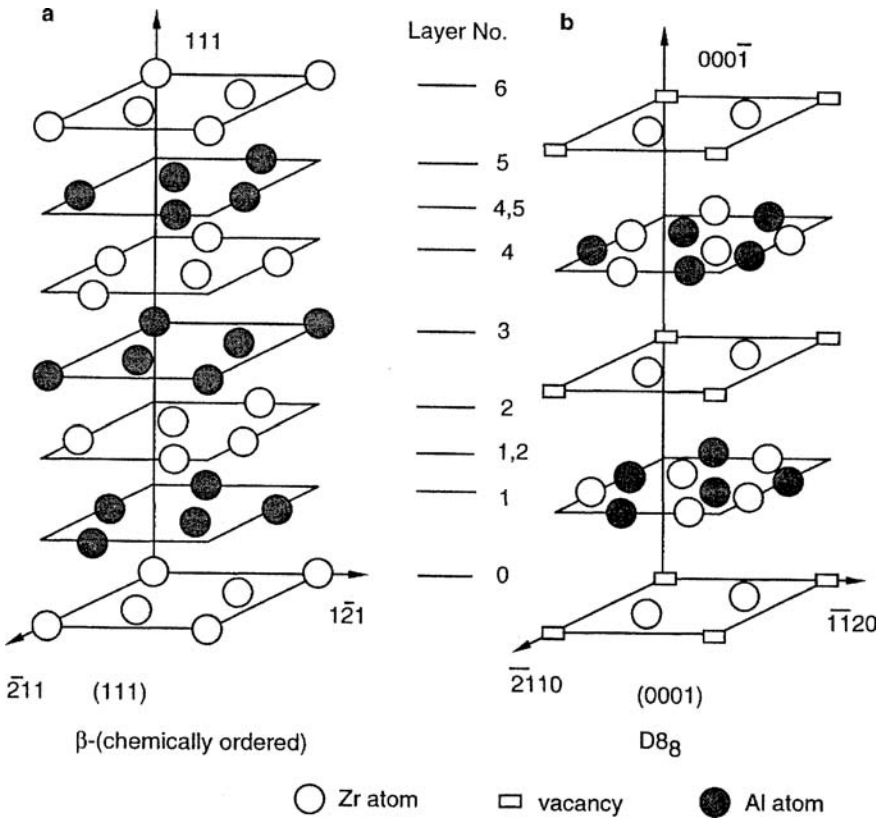

Fig. 17. Lattice correspondence between the ordered bcc (B2) and the $D8_8$ structures. The collapse of {222} planes of the bcc structure (designated as 1 and 2 or 4 and 5) at the intermediate positions (designated as 1, 2 or 4, 5) would produce the $D8_8$ structure. (a) The atomic arrangement in the B2 unit cell. (b) The atomic arrangement in the $D8_8$ unit cell.

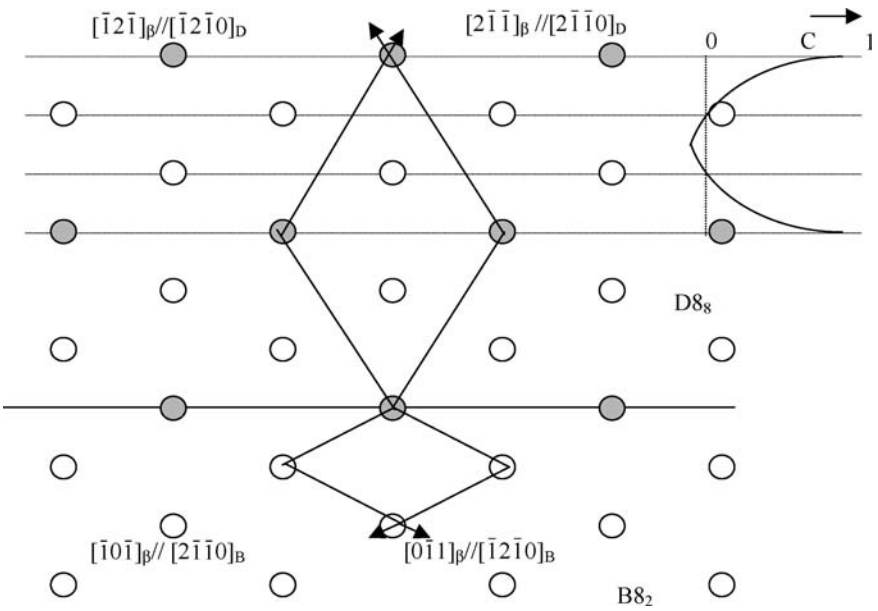

Fig. 18. Schematic representation of the basal planes of the $D8_8$ and the $B8_2$ structures. Replacing the vacancies in the basal planes of the $D8_8$ structure converts the $D8_8$ structure into the $B8_2$ structure.

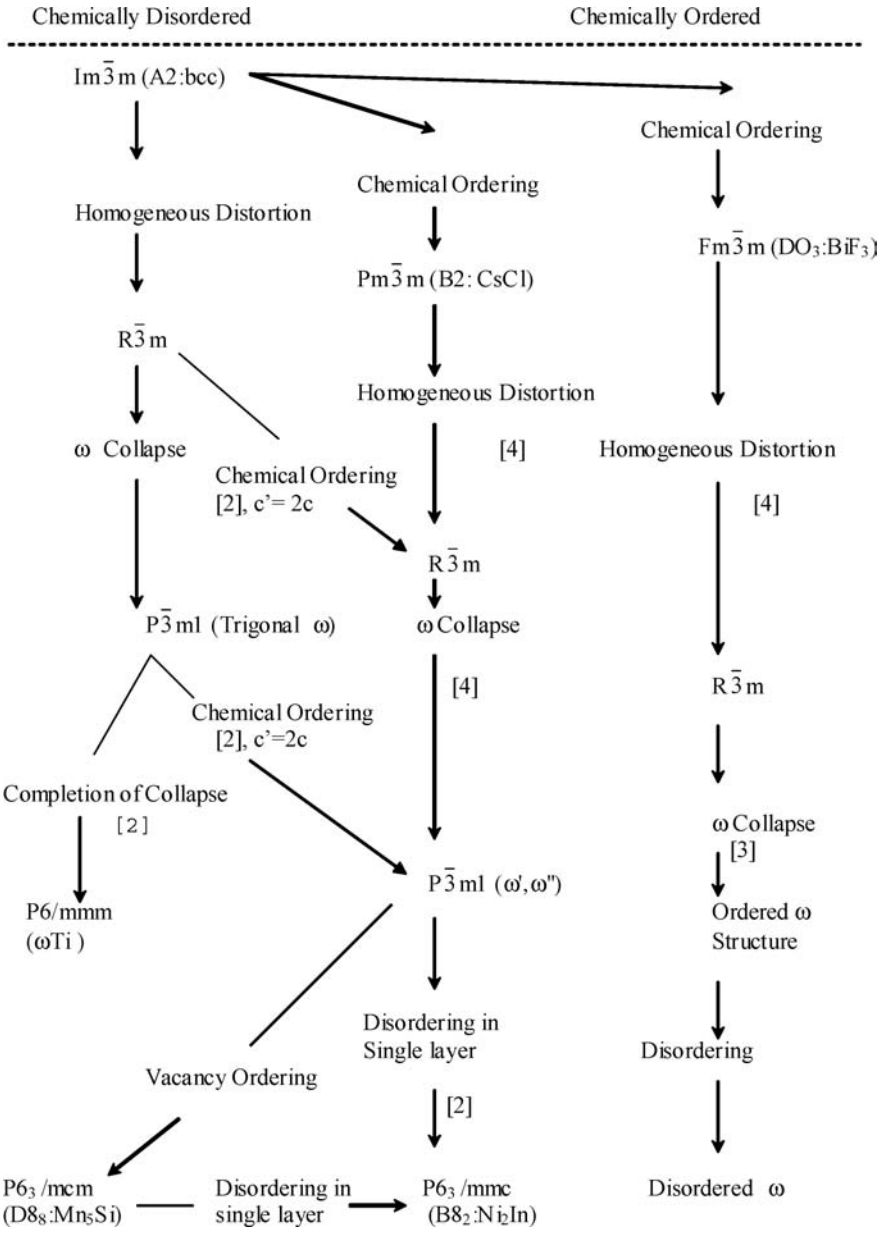

Fig. 19. Symmetry tree representation of phase transformations of $\beta \rightarrow \omega$ related phases. The bold lines represent the sequence of phase transformations observed in the Zr_3Al based alloys whereas the other sequences of phase transformations are reported in the literature.

Table 2. Mechanism of formation of the ω phase.

Treatment	Morphology	Size	Nature	Composition	Mechanism
Quenching from the β phase field	Ellipsoidal	Ranging from 2–10 nm	Athermal	Compositional invariant	Shuffle dominating
Isothermal aging	Ellipsoidal or cuboidal	Ranging from 10–20 nm	Isothermal	Compositional variant	Long range diffusion and shuffle
Static Pressurization	Fine particle to grain size	Ranging from few nm to few μm	Isothermal	Composition invariant/invariant (can occur in pure elemental form in Zr, Ti and Hf)	Atomic jump involved
Shock Pressurization	Plate shape morphology	Few μm	Athermal (nearly)	Compositional invariant	Shear dominating
Irradiation	Particulate morphology	Ranging from 1–5 nm	Isothermal	Compositional invariant	Radiation enhance precipitation and diffusion Shuffle + atomic Jump

displacement ordering and accompanying chemical ordering by coupled displacive-replacive ordering processes (Fig. 19).

5. Concluding remarks

The ω phase transformation forms an interesting class of transformation. The lattice collapse mechanism, which involves the 2/3<111> longitudinal displacement wave to produce ω lattice from the bcc lattice, is shown to be operative in nearly all the cases of the $\beta \rightarrow \omega$ phase transformation. The ω phase can be induced in various morphologies. The observed dual phase $\beta + \omega$ structure and the fine particle morphology can be explained in terms of the small difference between the $\boldsymbol{K}_m$ and $\boldsymbol{K}_\omega$ vectors giving rise to the modulated structures.

The progressive development of the ω displacement wave during isothermal heat treatment is preceded by the solute partitioning, though the lattice collapse mechanism is still operative. This point is demonstrated from the in situ formation of the ω phase at a relatively low temperature under irradiation.

Under high pressure, the formation of ω occurs due to a volume change associated with the transformation. The platelet morphology of the ω phase observed in the shock-loaded experiment in Zr-20Nb alloy is due to the dominance of shear involved during transformation in a way similar to the martensitic transformation. The phenomenological theory of martensite can be successfully applied to predict the habit plane between the parent β and the product ω phase.

The formation of the ordered ω structures from the parent β-based phases can be described by a coupled displacive–replacive ordering process in which the displacive wave is longitudinal and the lattice collapse sequence is identical to that in the $\beta \rightarrow \omega$ transformation. The changes in the symmetries associated with these transformations can be represented in form of a symmetry tree.

Different morphologies of the ω phase observed under various conditions are summarized in Table 2.

References

[1] P.D. Frost, W.M. Parris, L.L. Hirsh, J.R. Doig, C.M. Schwartz: Trans. Am. So. Metals. 46 (1954) 231.
[2] J.C. Jamison in: Metallurgy at High Pressures and Temperature, K.A. Gschneidner Jr., M.T. Hepworth, N.A.D. Parlee (Eds.), Gorden and Breach, New York (1964) 201.
[3] S.K. Sikka, Y.K. Vohra, R. Chidambaram: Prog. Mater. Sci. 27, (1982) 245.
[4] B.S. Hickman: Trans. TMS-AIME 242 (1969) 2461.
[5] J.C. Williams, D. DeFontaine, N.E. Paton: Metall. Trans. 4 (1973) 2701.
[6] W. Sinkler, D.E. Luzzi: Acta Metall. Mater. 42 (1994) 1249.
[7] D. DeFontaine, N.E. Paton, J.C. Williams: Acta Metall. 19 (1971) 1153.
[8] S.L. Sass: J. Less Comm. Metals. 28 (1972) 157.
[9] C. Stassis, J. Zarestky, N. Wakabayashi: Phys. Rev. Lett. 41 (1978) 1726.
[10] G.K. Dey, R.N. Singh, R. Tewari, D. Srivastava, S. Banerjee: J. Nucl. Mater. 224 (1995) 146.
[11] L.A. Bendersky, W.J. Boettinger, B. Burton, F.S. Biancaniello, C.B. Shoemaker: Acta Metall. 38 (1990) 931.
[12] J.M. Silcock, M.H. Davies, H.K. Hardy: Symposium on the Mechanism of Phase Transformations in Metals, Institute of Metals. London (1955) 93.
[13] Yu.A. Bagaryatskiy, G.I. Nosova: Fiz. Metal. Metalloved 13 (1962) 415.
[14] R.F. Hehemann in: Proceedings of USAEC Symposium on Zirconium Alloy Department, GEAP-4089, L10 (1962).
[15] R.S. Nelson, J.A. Hudson, D.J. Mazey: J. Nucl. Mater. 44 (1972) 318.
[16] K. Nutall, D. Faulknar: J. Nucl. Mat. 67 (1977) 131.
[17] O.G. Hernandez, D.I. Potter, in: J.R. Holland, L.K. Mansur (Eds.), Phase Stability During Irradiation, The Metallurgical Society of AIME, (1978) 601
[18] P.W. Bridgman: Proc. Am. Acad. Art Sci. 81 (1952) 165.
[19] G. Jyoti, K.D. Joshi, S.C. Gupta, S.K. Sikka, G.K. Dey, S. Banerjee: Phil. Mag. Lett. 75 (1997) 291.
[20] L.M. Hsiung, D.H. Lassila: Acta Mater. 48 (2000) 4851.
[21] G.K. Dey, R. Tewari, S. Banerjee, G. Jyoti, S.C. Gupta, K.D. Joshi, S.K. Sikka: Acta Mater. 52 (2004) 5243.
[22] J.M. Sanchez, D. DeFontaine: Acta Metall. 26 (1978) 1083.
[23] W. Lin, H. Splat, B.W. Batterman: Phys. Rev. B 13 (1978) 5158.

[24] D. Schryvers, L.E. Tanner: Mater. Sci. Forum 56–58 (1990) 329.
[25] H.E. Cook: Acta Metall. 21 (1974) 1445.
[26] W. Sinkler, D.E. Luzzi: Acta Metall. Mater. 42 (1994) 1249.
[27] S. Banerjee, R.W. Cahn: Acta Metall. 31 (1983) 721.
[28] J.W. Christian: The Theory of Transformation in Metals and Alloys, Pergamon Press, Oxford, 1965.
[29] A.F. Acton, M. Bevis: Mater. Sci. Eng. 5 (1969/70) 19.
[30] M.P. Usikov, V.A. Zilbershtein: Phys. Status Solidi A 19 (1973) 53.
[31] Y.K. Vohra: Acta Metall. 27 (1979) 1671.
[32] A. Rabinkin, M. Talianker, O. Botstein: Acta Metall. 29 (1980) 691.
[33] S.G. Song, G.T. Gray: Phil. Mag. 71A (1995) 275.
[34] P. Georgopoulos, J.B. Cohen: Acta Metall. 29 (1980) 1053.
[35] A. Prasetyo, F. Reynaud, H. Warlimont: Acta Metall. 24 (1976) 1009.
[36] S. Banerjee, R. Tewari, P. Mukhopadhyay: Prog. Mater. Sci. 42 (1997) 109.
[37] R. Tewari, P. Mukhopdyay, S. Banerjee, L.A. Bendersky: Acta Mater. 24 (1999) 1307.
[38] L.A. Bendersky, W.J. Boettinger, B.P. Burton, F.S. Biancaniello: Scripta Metall. 24 (1990) 1541.

(Received January 24, 2006; accepted April 22, 2006)

Correspondence address

Dr. Raghvendra Tewari
Materials Science Division
Bhabha Atomic Research Centre, Mumbai 400 085, India
Tel.: +91 22 255 93813
Fax: +91 22 255 05151
E-mail: rtewaribarc@yahoo.co.in